Redirecting on-surface cycloaddition reactions in a self-assembled ordered molecular array on graphite

Yu Li Huang,*[1,6] Ke Yang,[2,6] Jing Yang,[3,6] Sisheng Duan,[4] Yihe Wang,[1,5] Mingyue Sun,[1,4] Yong-Wei Zhang,*[2] Ming Yang,*[2] and Andrew T. S. Wee[4]

[1]Joint School of National University of Singapore and Tianjin University, International Campus of Tianjin University, Binhai New City, Fuzhou, 350207, China

[2]Department of Applied Physics, The Hong Kong Polytechnic University, Kowloon, Hong Kong SAR, China

[3]Institute of High Performance Computing (IHPC), Agency for Science, Technology and Research (A*STAR), 1 Fusionopolis Way, #16-16 Connexis, Singapore 138632, Republic of Singapore

[4]Department of Physics, National University of Singapore, Singapore 117542, Singapore

[5]Department of Chemistry, National University of Singapore, Singapore 117543, Singapore

[6]These authors contributed equally to this work.

*Corresponding Authors: hyl@tjufz.org.cn, zhangyw@ihpc.a-star.edu.sg, kevin.m.yang@polyu.edu.hk

Abstract

The synthesis of atomically precise carbon nanostructures in ultra-high vacuum has seen extensive progress on metal surfaces. However, this remains challenging on chemically inert surfaces. It is because the thermally activated C-C coupling encounters a severe "desorption problem" on weakly interacting substrates. Here, we report an extraordinary [2+2+2+2] cycloaddition occurring in a highly ordered π-conjugated molecular array on graphite, via Fe-mediated dehydrohalogenative reactions. This is in contrast to the dehalogenative [2+2] cycloaddition reactions previously reported on noble metal surface. More interestingly, various products are observed and embedded in the close-packing supramolecular arrays as defective individuals or chains (grain boundaries). First-principles calculations reveal that the energy barriers of the multiple dehalogenation, dehydrogenation, and cycloaddition reactions are reduced by catalytic Fe atoms but remain energetically unfavorable. As thus, additional intermolecular

coupling, steric hindrance, and/or interfacial interactions could play significant roles on redirecting the on-surface synthesis on non-metal substrates.

Introduction

On-surface synthesis in ultrahigh vacuum (UHV) has garnered intensive interest as a promising approach to fabricate atomically precise organic nanostructures with tunable functionality.[1-3] In particular, surface-assisted dehalogenative and dehydrogenative cycloaddition reactions, stemming from the conventional Ullmann coupling, have predominantly been showcased on noble metal surfaces. These reactions have generated a variety of complex π-conjugated structures, including nanographenes,[4-6] carbon nanoribbons,[7, 8] and others.[9] It is well understood that the metal substrates not only serve as a surface for hosting the precursors, intermediates, and final products, but also provide metal catalytic agents for the reactions and even constituents of organometallic intermediates.[10-12] Thus, the reaction pathways, activation barriers, and product outcomes may vary significantly on different metal surfaces using the same precursor.[11, 13] Furthermore, metal substrates could strongly screen the intrinsic properties of the designed nanostructures and might limit their applications.[14-18]

Much work has also been devoted to the on-surfaces synthesis on non-metal substrates.[17, 19-21] Various strategies have been developed to facilitate chemical reactions on substrates such as rutile TiO_2,[22, 23] calcite $CaCO_3$,[24] mica,[25] NaCl,[26, 27] and even single-layered graphene[28] and boron nitride (BN)[29] on metal surfaces, assisted by pre-designed precursors, guest catalytic agents, photocatalysis, or tip manipulations under vacuum conditions. In particular, chemically inert graphite has been widely used in traditional in-solution synthesis of two-dimensional (2D) covalent organic frameworks via reversible condensation reactions,[19, 30-34] as well as mesoscale photopolymerization in UHV.[35] Graphite is also highly desirable for precisely characterizing the intrinsic properties of on-surface synthesized nanostructures, benefiting from its atomical flatness and electronic decoupling. However, thermally activated C-C recombination in UHV remains elusive on such an inert substrate due to the "desorption problem".[19] This arises when the reactants prematurely desorb from the surface before the reaction can occur, which depends on the delicate balance between the reaction barrier and the desorption threshold. Moreover, the underlying reaction mechanism on such a chemically inert surface may distinctly differ from the extensively studied metal

surfaces, presenting opportunities for further investigation.

Here we present the realization of Fe-assisted cycloaddition reactions within a close-packed, highly ordered supramolecular array assembled on a graphite surface via mild annealing. 2,3,6,7,10,11-hexabromotriphenylene (HBTP) is chosen as the precursor due to its relatively low dehalogenative reaction barrier.[13, 36] As illustrated in Figure 1a, upon adsorption of HBTP molecules on Ag(111), debromination reactions can occur below room temperature, facilitated by the Ag adatoms to form organometallic intermediates. Subsequent annealing at temperatures ranging from 420 – 560 K leads to final [2+2] cycloaddition products by removing the Ag adatoms from the intermediates. Using low-temperature scanning tunneling microscopy (LT-STM), an extraordinary [2+2+2+2] cycloaddition reaction (Figure 1b) catalyzed by Fe guest atoms[37-39] is identified in the well-ordered HBTP supramolecular array on graphite, via multiple dehalogenative and dehydrogenative reactions. The reactions further demonstrate a domino-like fashion among homo-species to form one-dimensional (1D) grain boundaries (GBs), which are facilitated by the side-by-side intermolecular coupling and steric hindrance. Furthermore, density functional theoretical (DFT) calculations propose a possible reaction pathway, suggesting that the Fe atoms also play significant roles in anchoring the intermediates and products. This study offers new insights into the metal-mediated on-surface synthesis on inert substrates and presents a promising route to fabricate diverse carbon-based nanostructures.

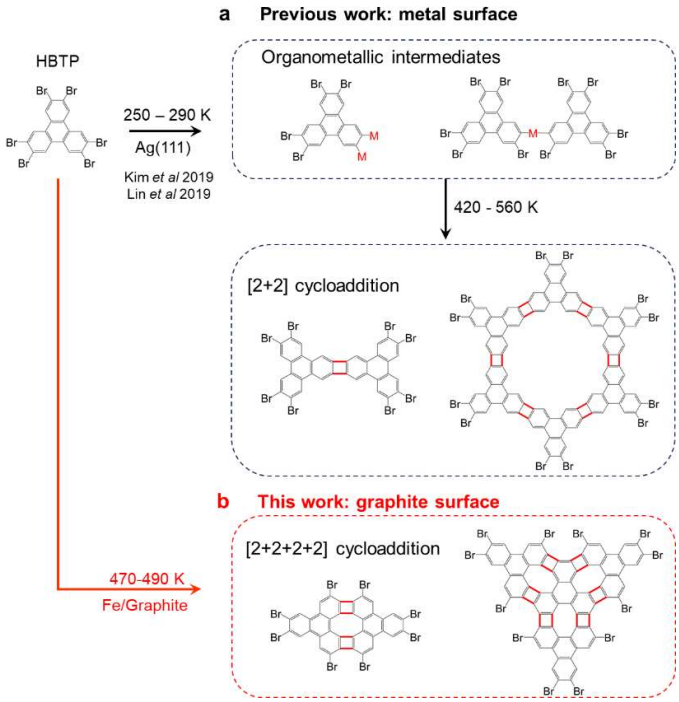

Figure 1. Cycloaddition reactions of HBTP molecules on different substrates. (a) Stepwise [2+2] cycloaddition reactions previously reported on Ag(111) with the presence of various organometallic intermediates [from Ref. 13, 36]. (b) [2+2+2+2] cycloaddition reactions assisted by Fe catalytic agent via complicated dehalogenative and dehydrogenative reactions on graphite in this work.

Results and Discussion

Figure 2a depicts a self-assembly of HBTP monolayer on a graphite surface in (50×50 nm^2), where highly ordered, close-packed supramolecular arrays are formed with domain sizes extending over hundreds of nanometers. Upon closer inspection in Figure 2b, each HBTP molecule is discernible as a trefoil feature. It is found that under positive tip voltages (V_{tip}), the occupied states of the HBTP molecules located at its three peripheral aromatic rings (Figure S1 in supporting information, SI). The unit cell is highlighted by a yellow rhombus, with experimental lattice constants of a = b = 1.24 ± 0.02 nm and γ = 59° ± 2°. These values are consistent with the DFT optimized supramolecular structure on graphite (see DFT calculations in SI) shown in Figure 2c, where a = b = 1.23 nm and γ = 60°. The intermolecular Br-Br distance is 3.60 Å, aligning with previously reported values.[40, 41] This HBTP supramolecular array is mainly stabilized via the molecule-substrate π-π coupling and intermolecular halogen bonding. Furthermore, it is worth noting that the assembly of achiral molecules on

surfaces can induce chirality.[42, 43] The right (R) configuration is depicted in Figure 1c, and evidenced by Figure 1b and 1d. Examples of the left (L) ones can be found in Figure 1e and Figure S4.

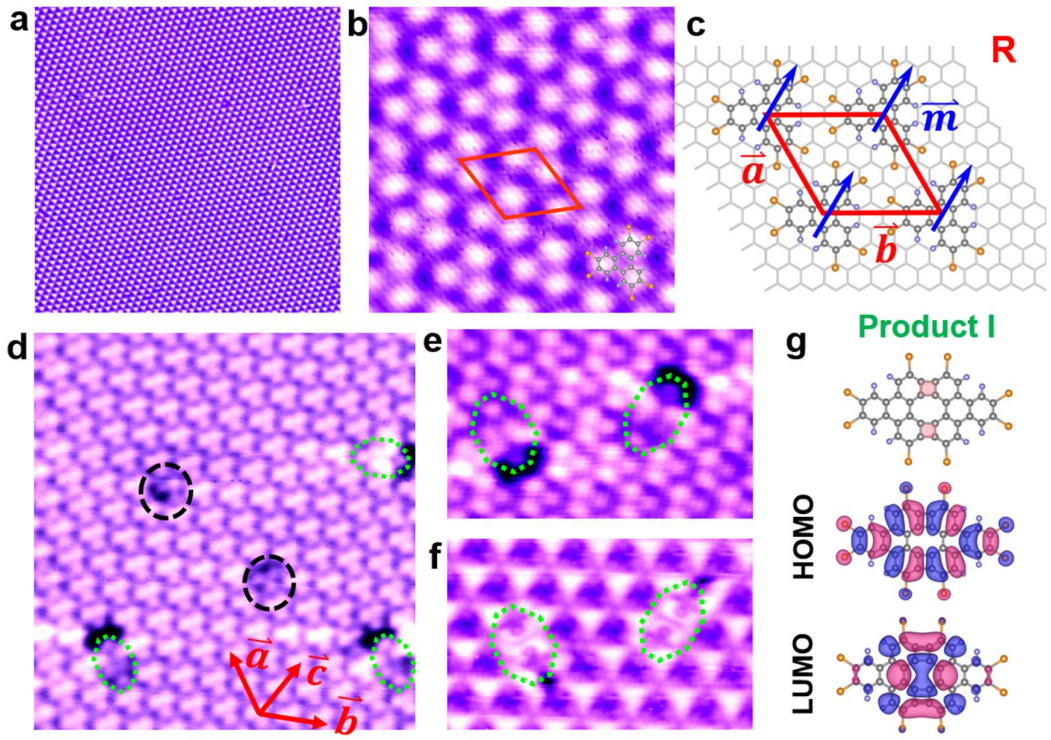

Figure 2. [2+2+2+2] cycloaddition reactions occurred in the highly-ordered HBTP supramolecular arrays. (a) Large-scale STM image of the highly-ordered, close-packed HBTP monolayer on graphite surface (50×50 nm^2; V_{tip} = -2.5 V, I = 40 pA). (b) Zoom-in topographic image revealing the trefoil feature of each HBTP molecule (5×5 nm^2; V_{tip} = 3.0 V, I = 30 pA). (c) The DFT optimized HBTP unit cell with right configuration on graphite. (d) Various 'defective' molecules are observable in the HBTP supramolecular arrays after dosing a few Fe atoms and annealing at 210°C (15×15 nm^2; V_{tip} = 3.0 V, I = 40 pA). (e) Occupied state of the product **I** (green polygons) formed by [2+2+2+2] cycloaddition recorded at V_{tip} = 3.4 V, and **f**, unoccupied state recorded at V_{tip} = -2.5 V, respectively (e and f, 8×5 nm^2; I = 80 pA). (g) Optimized structural model of the product **I**, and the corresponding HOMO and LUMO states (isoface = 0.01 e Å^{-3}). In panel (c) and (g), C atoms in the HBTP molecule and graphite are in dark and light grey, respectively; H and Br atoms are in cyan and gold, respectively.

Subsequently, Fe atoms were thermally evaporated onto the HBTP monolayer to trigger possible dehalogenative cycloaddition reactions (Experimental methods in SI). When a little amounts of Fe atoms (~0.01 ML) were dosed onto the HBTP arrays by holding the sample at 210°C, many defective molecules are observable in Figure 2d. They can be divided into two categories. The first species are highlighted by black

dashed circles, which retain the trefoil shapes with dim contrast. These are likely to be partially debrominated HBTP molecules, which had been previously reported on metal substrates.[13, 36] Such molecules can also be found in the as-grown HBTP monolayer after annealing at 200°C without Fe catalyst (Figure S5).

The second species (product **I**) appear as spindle-like shapes, as highlighted by green polygons in Figure 2d, which can be easily distinguished from the surrounding HBTP molecules by its two-fold symmetry. Obviously, it is completely different from the [2+2] cycloaddition products with dog-bone-shapes.[13, 36] Here, the highly ordered HBTP supramolecular array is well preserved with the embedded product **I**, whose long axis is parallel to the $\vec{a}$, $\vec{b}$, and $\vec{c}$ orientations of the molecular arrays. Figure 2e and 2f represent the occupied and unoccupied states of this new species recorded by STM at V_{tip} = 3.4 eV and V_{tip} = -2.5 eV, respectively. The possible supramolecular structure of the product **I** could be deduced by superimposing the benzenoid backbones of the HBTP molecules onto the molecularly resolved STM images (Figure S7). The proposed molecular model is depicted in Figure 2g, formed by two HBTP molecules fused together via complicated dehalogenation, dehydrogenation, and side-by-side [2+2+2+2] cycloaddition reactions. The calculated highest occupied molecular orbital (HOMO) and lowest unoccupied molecular orbital (LUMO) of the proposed model are in good agreement with the observed occupied (Figure 2e) and unoccupied states (Figure 2f) captured in STM images. In contrast, the head-to-head [2+2] cycloaddition reactions (Figure 1a) previously observed on metal substrates[13, 36] are absent here, and the possible reasons will be discussed later. Many other possible products were also proposed for comparison in Figure S1-S3.

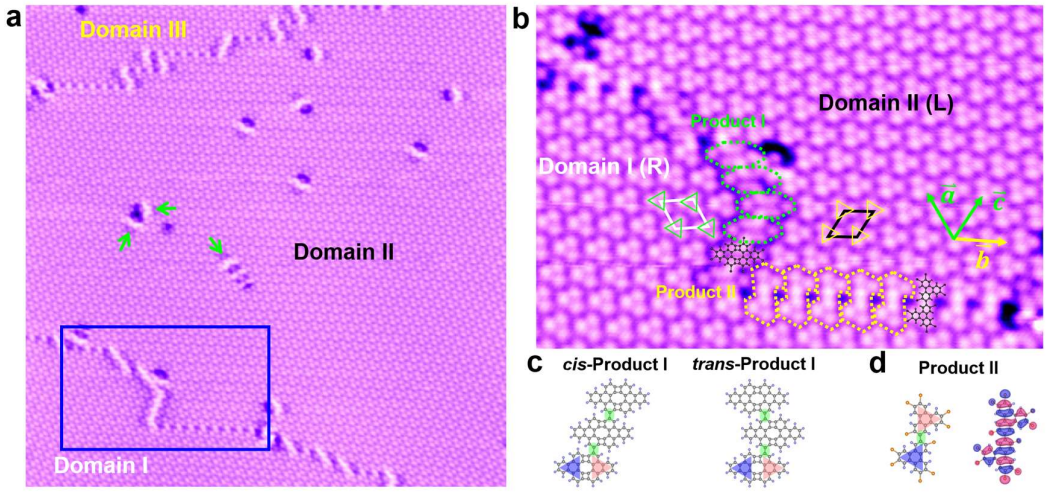

Figure 3. 1D GB constructed by 'defective' molecules. (a) Multiple domains with different molecular orientations are observed with the formation of 1D GBs (50×50 nm^2; V_{tip} = 3.0 V, I = 40 pA). The green arrows indicate three product **I** individuals along different orientations. (b) Enlarged STM image revealed that the GBs are composed by product **I** and **II** along $\vec{a}/\vec{c}$ and $\vec{b}$, respectively (14×20 nm^2; V_{tip} = 3.4 V, I = 50 pA). The black benzenoid backbones of the product **I** and **II** are superimposed for guiding eyes. (c) The schematic models of cis-product **I** and trans-product **I**. (d) Optimized structural model and calculated HOMO of product **II**. The green shadows highlight the intermolecular dehalogenations.

More dehalogenative products were obtained by increasing the Fe doses to ~0.1ML (Figure 3). Interestingly, 1D GBs constructed by defective-like molecules are observed in Figure 3a. Meanwhile, individual products **I** are randomly distributed within the molecular domains as indicated by the green arrows. Figure 3b represents a close-up of the GBs, enlarged from the region highlighted by a blue rectangle in Figure 3a. The unit cells of domain I and II are marked by white and black rhombuses, respectively, revealing the chirality induced upon adsorption. The GBs are formed along the highest symmetric orientations of the molecular array, i.e., $\vec{a}$, $\vec{b}$, and $\vec{c}$, with intersection angles of 60°. Interestingly, the basic building blocks of the GBs along $\vec{b}$ ($GB_{\vec{b}}$) are distinctly different from the other two along $\vec{a}$ ($GB_{\vec{a}}$) and $\vec{c}$ ($GB_{\vec{c}}$). In the $GB_{\vec{a}}$ and $GB_{\vec{c}}$, the building units highlighted by green spindle-like shapes are similar to product **I**. That is, GBs along $\vec{a}$ and $\vec{c}$ are both constructed by 1D *cis*-product **I** chains via intermolecular C-C coupling, after debrominations at the sites denoted by green shadow in Figure 3c. Meanwhile, *trans*-product **I** emerges at the intersection of the $GB_{\vec{a}}$ and $GB_{\vec{c}}$ (Figure S8a). In contrast, the building block of $GB_{\vec{b}}$ is identified as product **II** with a dumbbell-

shape, formed by a pair of debrominated HBTP molecules as shown in Figure 3d. The benzenoid backbones of the product **I** and **II** are superimposed in Figure 3b for guiding eyes.

The formations of such 1D GBs suggest that the dehalogenative and dehydrogenative C-C coupling can occur in a domino-like fashion,[20] and the steric hindrance effect could play significant roles. It can be seen that the neighboring HBTP molecules across the $GB_{\vec{a}}$ and $GB_{\vec{c}}$ are packing in a side-to-side manner (Figure S1), thus facilitating the [2+2+2+2] cycloaddition reactions to form products **I**. While across the $GB_{\vec{b}}$, the neighboring molecules are aligned in a head-to-head manner (Figure S1) to form products **II**. In fact, the irregular GBs are mixtures of products **I** along $GB_{\vec{a}}$/$GB_{\vec{c}}$ and products **II** along $GB_{\vec{b}}$ (Figure S8a). The length of the regular $GB_{\vec{a}}$ or $GB_{\vec{c}}$ composed by cis-product **I** can extend over tens of nanometers, e.g., ~30 nm (Figure S8b). The GBs divide the large, homogeneous domains with single packing configuration into small, heterogeneous domains with mirror-symmetric configurations.

Close-packed supramolecular islands extending over 100 nm persist on the graphite surface even with more than 30% products (Figure S9). As shown in Figure 4a, when the total products reach ~30%, HBTP molecular domains decrease to several nanometers only, and larger supramolecules or even polymers based on the product **I** and **II** are formed. For instance, Figure 4b demonstrates a trimer **I** formed by simple dibrominated C-C coupling (highlighted by red bonds), derived from product **II**; while Figure 4c and 4d show a trimer II and a tetramer respectively, derived from product **I** via multiple [2+2+2+2] cycloadditions (red bonds). Furthermore, trimer **I** and **II** can be considered as new types of GBs, where the molecules in the upper and bottom domains separated by these trimers possess the same orientation. More examples are given in Figure S9.

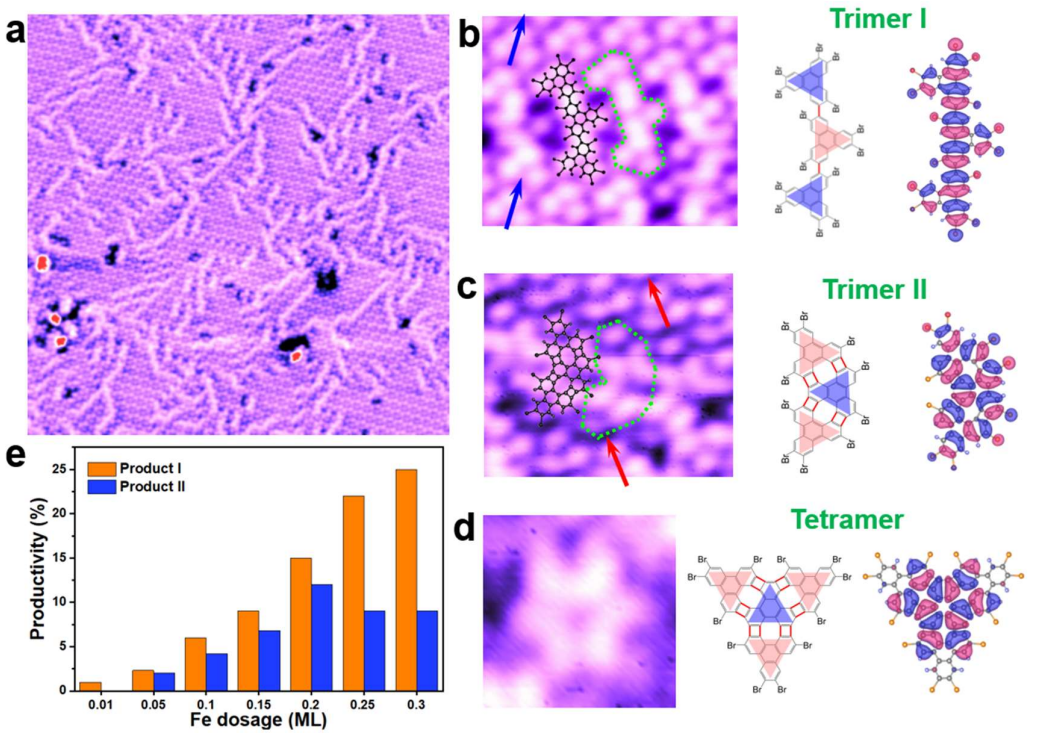

Figure 4. Products at high Fe dosage (~0.3 ML). (a) The formation of close-packed molecular domains with a high density of reaction products and dendritic GBs (50×50 nm^2; V_{tip} = 3.0 V, I = 10 pA). (b-d) Left: STM images of trimer **I** (b), trimer **II** (c), and tetramer (d) (b, 5.5×4.5 nm^2; V_{tip} = 3.0 V, I = 80 pA; c, 5.4×4.4 nm^2; V_{tip} = 3.0 V, I = 20 pA; d, 2.7×2.7 nm^2; V_{tip} = 2.6 V, I = 10 pA). Middle: the corresponding molecular models. Right: the corresponding HOMO states. (e) Statistical productivities of product **I** and **II** with the increasing Fe dosages. Each dosage was statistically analyzed over 1000-2000 molecules.

Consequently, we analyze the productivities of product **I** and **II** under various Fe dosages in Figure 4e, which quantitatively increase with the Fe dosages. Products **I** can be obtained as individuals at extremely low Fe dosage (e.g., ~0.01 ML) (Figure 2), while products **II** are found at GBs as the dosage increases to ~0.05 ML (Figure 3). Overall, the product **I** (golden column) increases faster and dominates over the product **II**, and its productivity can reach as high as ~25% within the investigated range. In contrast, the productivity of product **II** (blue column) reaches its maximum at ~12% at ~0.2 ML, and almost saturate at ~10% with even higher Fe dosages. This observation seems anomalous, as the formation of product **I** involves much complicated debromination, dehydrogenation and recombination processes, while product **II** only requires debromination and C-C bonding processes. The underlying mechanisms are explored in below.

To simulate the formation processes of product **I** on the graphite substrate, we divide the reactions into five possible steps: 0) Fe-assisted debromination; 1) the 1st

dehydrogenation; 2) the 2nd dehydrogenation; 3) desorption of two HBr molecules; and 4) [2+2+2+2] cycloaddition. Firstly, DFT calculation results suggest that the step 0), debromination, is exothermic (Figure S10). This implies that debromination could occur spontaneously upon capturing Fe atoms near the HBTP molecule. Additionally, it is found that the single HBPT molecule interacts weakly with graphite via van der Waals forces, while the Fe atom acts as an anchor, firmly fixing the HBPT on the surface, thus facilitating the subsequent reactions. Subsequently, in the step 1), the configuration 0 in Figure 5c is formed by two Fe atoms bridging the debrominated HBTP (debr-HBTP) molecule and the Br atoms, due to the spontaneous breakage of the C-Br bonds. In the following, one C-H bond next to the debromination site is activated and broken, forming an HBr molecule adsorbed nearby the Fe atom (configuration 5 in Figure 5c). This process repeats again in the step 2) to form the 2nd HBr molecule (Figure 5d). Figure 5a reveals that the energy barrier for the 1st dehydrogenation (configuration 0-5) is 1.23 eV (Δ_1), which slightly increases to 1.42 eV (Δ_2) for the 2nd one (configuration 5-10) due to the positively charged HBTP molecule. After these two steps, the debrominated and dehydrogenated HBTP (debr-dehy-HBTP) molecule is still anchored on the graphite surface via the Fe atoms, and the two HBr molecules are physisorbed, as demonstrated in configuration 10, Figure 5d. In the step 3), these two HBr molecules could diffuse away from the reaction sites (Figure 5e) via a small energy barrier of 0.68 eV (Δ_3), which indicates the possibility of releasing at even room temperature (a barrier of ~30 $k_BT \approx 0.77$ eV). In the final step 4), two debr-dehy-HBTP molecules are placed side-to-side for the [2+2+2+2] cycloaddition (configuration 0 in Figure 5f). These two molecules could spontaneously slide closer to each other (configuration 0 to 3 in Figure 5f), which is exothermic as revealed by Figure 5b. Then the recombination of the first pair of C-C bonds (configuration 3 to 4 in Figure 5f), namely the first half of the [2+2+2+2] cycloaddition, is endothermic with an energy barrier of 0.72 eV (Δ_4), while the second half of the [2+2+2+2] cycloaddition (configuration 4 to 6 in Figure 5f) is exothermic.

According to this proposed step-by-step reaction pathway, the highest energy barrier to be overcome is the 2nd dehydrogenation, namely $\Delta_2 = 1.42$ eV, which is possible upon mild annealing at ~210℃. Indeed, this temperature is relatively low compared to that usually required to active dehydrogenation and/or eliminate organometallic intermediates on metal substrates.[10, 22, 36, 44, 45] Furthermore, the side-views of all these

configurations discussed in Figure 5c-f are shown in Figure S11. It is worth noting that the Fe atoms are bonding with all the intermediates/products and the graphite substrate to increase the stability. In particular, after the [2+2+2+2] cycloaddition reactions, the Fe atoms are sandwiched between product **I** and graphite as shown in Figure 5f and Figure S11d. Further MD calculations demonstrates that the Fe atoms could escape within 5 ps at 600 K (Figure S12). In fact, many $FeBr_x$ clusters and domains are observable at the edges of the molecular islands after annealing (e.g., Figure S6e and Figure S8b).

We also calculated the possible reaction pathways of the product **II**. The formation of product **II** only requires the breaking of a single C-Br bond and the recombination of a C-C bond, with relatively low energy barriers of 0.83 eV and 0.58 eV, respectively (Figure S13). Usually, the productivities depend on the activation energies, the lower the energy barrier, the higher the productivity. Thus, it is unusual that the products **I** are always more than the products **II**. One possible reason is that the product **I** is actually held by two de-Br-HBTP molecules at the sides via chemical coupling, namely product **I'** shown in Figure S1c and Figure S7. Such intermolecular coupling might not only enhance its stability on the graphite surface, but also reduce the reaction barrier to form product **I'**. Furthermore, the formation of individual product **II** is excluded in the highly order HBTP supramolecular arrays, possibly due to the steric hindrance effect.

Finally, possible pathways lead to the head-to-head [2+2] cycloaddition reactions (Figure 1a) were considered. As shown in Figure S14, the formation of the [2+2] cycloaddition involves two debrominations and two C-C bonding processes without dehydrogenation. However, the energy barriers for the 1^{st} and 2^{nd} C-C coupling in the [2+2] cycloaddition are as high as 3.05 eV and 1.94 eV, respectively. These barriers are much higher than that for the product **I**, making it reasonable of the absence of [2+2] cycloaddition. Such phenomena are distinct from those on intensively studied metal surface, where individual intermediates/products could strongly interact with the substrates, and the steric hindrance and intermolecular coupling are less significant.

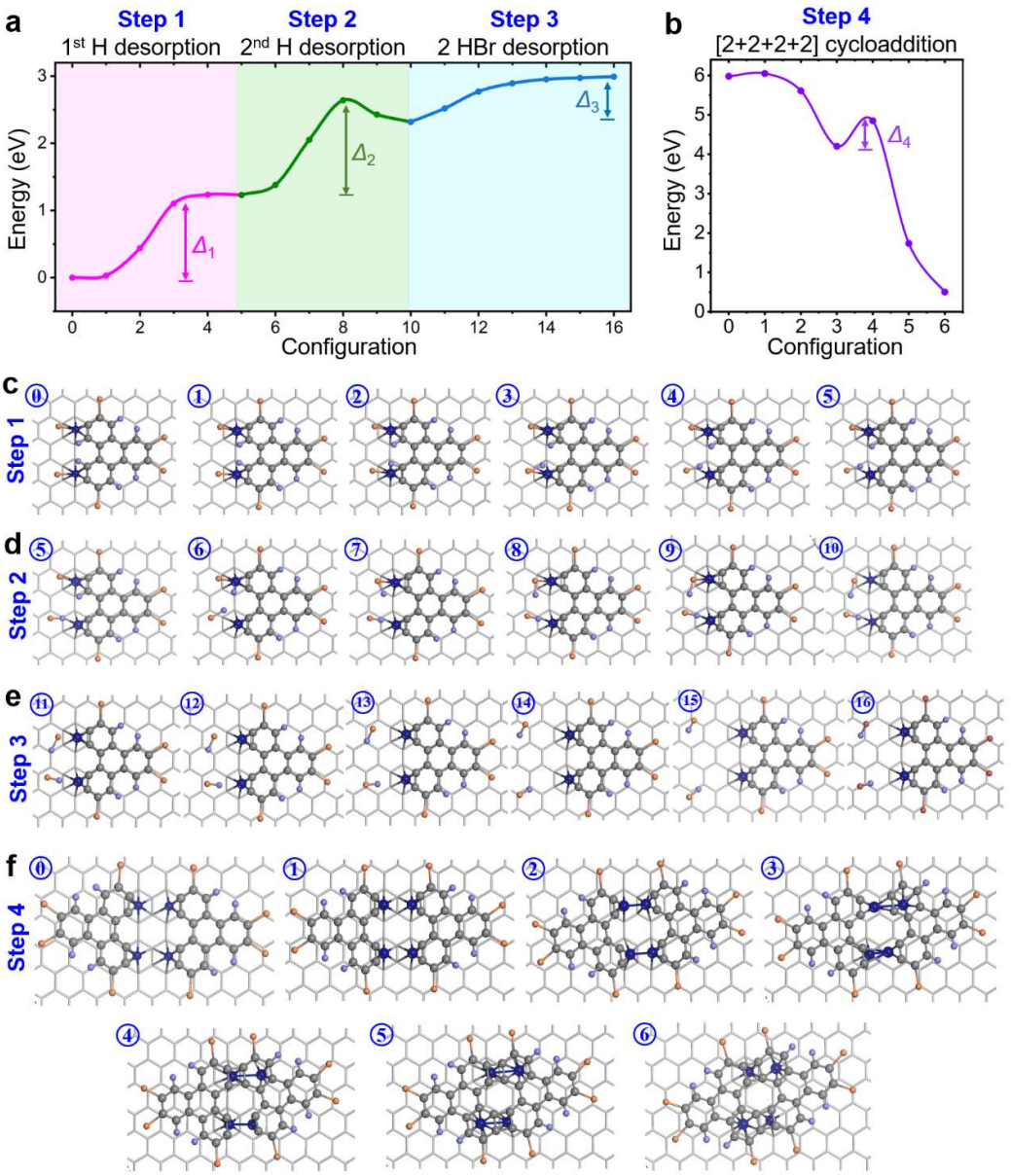

Figure 5 Possible reaction paths of the product I. (a) The energy profile of the dehydrogenations of the 1st (step 1) and 2nd (step 2) H atoms, and the desorption of the two HBr molecules (step 3) for a single HBTP molecule. (b) The energy diagram of the [2+2+2+2] cycloaddition of two debr-dehy-HBTP molecules (step 4). (c-f) The corresponding configurations of the possible transition states with local energetic minima of the step 1-4 in the panel (a) and (b). C atoms in the HBTP molecule and graphite are in dark and light grey, respectively; H, Br and Fe atoms are in cyan, gold and blue, respectively.

In conclusion, we have demonstrated the redirected on-surface synthesis on the chemically inert graphite surface, where [2+2+2+2] cycloaddition reactions are observed in the self-assembled HBTP molecular arrays via Fe-catalyzed

dehydrohalogenations. A variety of complex products are observed as the dosage of Fe catalytic agents increases, including product **I**, product **II**, and their derivates. Additionally, we conducted calculations to explore the possible reaction pathways of the products **I** and **II**, as well as the excluded [2+2] cycloadditions. It suggests that the formation of the major product **I** via [2+2+2+2] cycloaddition could be facilitated by additional intermolecular coupling, steric hindrance, and/or interfacial interactions. These findings reveal the emergence of entirely different products and a distinct reaction mechanism and on graphite. This study could serve as a prototype model for the on-surface synthesis on weakly interacting substrates, opening a new access to engineer carbon-based nanostructures.

Reference

(1) Grill, L.; Hecht, S. Covalent on-surface polymerization. *Nat Chem* **2020**, *12* (2), 115-130. DOI: 10.1038/s41557-019-0392-9 From NLM PubMed-not-MEDLINE.

(2) Houtsma, R. S. K.; de la Rie, J.; Stohr, M. Atomically precise graphene nanoribbons: interplay of structural and electronic properties. *Chem Soc Rev* **2021**, *50* (11), 6541-6568. DOI: 10.1039/d0cs01541e From NLM PubMed-not-MEDLINE.

(3) Clair, S.; de Oteyza, D. G. Controlling a Chemical Coupling Reaction on a Surface: Tools and Strategies for On-Surface Synthesis. *Chem Rev* **2019**, *119* (7), 4717-4776. DOI: 10.1021/acs.chemrev.8b00601 From NLM PubMed-not-MEDLINE.

(4) Treier, M.; Pignedoli, C. A.; Laino, T.; Rieger, R.; Mullen, K.; Passerone, D.; Fasel, R. Surface-assisted cyclodehydrogenation provides a synthetic route towards easily processable and chemically tailored nanographenes. *Nat Chem* **2011**, *3* (1), 61-67. DOI: 10.1038/nchem.891 From NLM Medline.

(5) Mishra, S.; Catarina, G.; Wu, F.; Ortiz, R.; Jacob, D.; Eimre, K.; Ma, J.; Pignedoli, C. A.; Feng, X.; Ruffieux, P.; et al. Observation of fractional edge excitations in nanographene spin chains. *Nature* **2021**, *598* (7880), 287-292. DOI: 10.1038/s41586-021-03842-3 From NLM PubMed-not-MEDLINE.

(6) Sanchez-Sanchez, C.; Nicolai, A.; Rossel, F.; Cai, J.; Liu, J.; Feng, X.; Mullen, K.; Ruffieux, P.; Fasel, R.; Meunier, V. On-Surface Cyclization of ortho-Dihalotetracenes to Four- and Six-Membered Rings. *J Am Chem Soc* **2017**, *139* (48), 17617-17623. DOI: 10.1021/jacs.7b10026 From NLM PubMed-not-MEDLINE.

(7) Huang, H.; Wei, D.; Sun, J.; Wong, S. L.; Feng, Y. P.; Neto, A. H.; Wee, A. T. Spatially resolved electronic structures of atomically precise armchair graphene nanoribbons. *Sci Rep* **2012**, *2*, 983. DOI: 10.1038/srep00983 From NLM Medline.

(8) Zhou, X.; Yu, G. Modified Engineering of Graphene Nanoribbons Prepared via On-Surface Synthesis. *Adv Mater* **2020**, *32* (6), e1905957. DOI: 10.1002/adma.201905957 From NLM PubMed-not-MEDLINE.

(9) Tran, B. V.; Pham, T. A.; Grunst, M.; Kivala, M.; Stohr, M. Surface-confined [2 + 2] cycloaddition towards one-dimensional polymers featuring cyclobutadiene units. *Nanoscale* **2017**, *9* (46), 18305-18310. DOI: 10.1039/c7nr06187k From NLM PubMed-not-MEDLINE.
(10) Zint, S.; Ebeling, D.; Schloder, T.; Ahles, S.; Mollenhauer, D.; Wegner, H. A.; Schirmeisen, A. Imaging Successive Intermediate States of the On-Surface Ullmann Reaction on Cu(111): Role of the Metal Coordination. *ACS Nano* **2017**, *11* (4), 4183-4190. DOI: 10.1021/acsnano.7b01109 From NLM PubMed-not-MEDLINE.
(11) Björk, J.; Hanke, F.; Stafström, S. Mechanisms of Halogen-Based Covalent Self-Assembly on Metal Surfaces. *Journal of the American Chemical Society* **2013**, *135* (15), 5768-5775. DOI: 10.1021/ja400304b.
(12) Bieri, M.; Nguyen, M.-T.; Groning, O.; Cai, J.; Treier, M.; Ait-Mansour, K.; Ruffieux, P.; Pignedoli, C. A.; Passerone, D.; Kastler, M.; et al. Two-Dimensional Polymer Formation on Surfaces: Insight into the Roles of Precursor Mobility and Reactivity. *J Am Chem Soc* **2010**, *132*, 16669-16676.
(13) Zhang, R.; Xia, B.; Xu, H.; Lin, N. Identifying Multinuclear Organometallic Intermediates in On-Surface [2+2] Cycloaddition Reactions. *Angew Chem Int Ed Engl* **2019**, *58* (46), 16485-16489. DOI: 10.1002/anie.201909278.
(14) Lyu, B.; Chen, J.; Lou, S.; Li, C.; Qiu, L.; Ouyang, W.; Xie, J.; Mitchell, I.; Wu, T.; Deng, A.; et al. Catalytic Growth of Ultralong Graphene Nanoribbons on Insulating Substrates. *Adv Mater* **2022**, e2200956. DOI: 10.1002/adma.202200956 From NLM Publisher.
(15) Blackwell, R. E.; Zhao, F.; Brooks, E.; Zhu, J.; Piskun, I.; Wang, S.; Delgado, A.; Lee, Y. L.; Louie, S. G.; Fischer, F. R. Spin splitting of dopant edge state in magnetic zigzag graphene nanoribbons. *Nature* **2021**, *600* (7890), 647-652. DOI: 10.1038/s41586-021-04201-y From NLM PubMed-not-MEDLINE.
(16) Jacobse, P. H.; Mangnus, M. J. J.; Zevenhuizen, S. J. M.; Swart, I. Mapping the Conductance of Electronically Decoupled Graphene Nanoribbons. *ACS Nano* **2018**, *12* (7), 7048-7056. DOI: 10.1021/acsnano.8b02770 From NLM PubMed-not-MEDLINE.
(17) Sun, K.; Fang, Y.; Chi, L. On-Surface Synthesis on Nonmetallic Substrates. *ACS Materials Letters* **2020**, *3* (1), 56-63. DOI: 10.1021/acsmaterialslett.0c00452.
(18) Jiang, S.; Neuman, T.; Boeglin, A.; Scheurer, F.; Schull, G. Topologically localized excitons in single graphene nanoribbons. *Science* **2023**, *379*, 1049–1053.
(19) Lackinger, M. Synthesis on inert surfaces. *Dalton Trans* **2021**, *50* (29), 10020-10027. DOI: 10.1039/d1dt00058f From NLM PubMed-not-MEDLINE.
(20) Ma, C.; Wang, J.; Ma, H.; Yin, R.; Zhao, X. J.; Du, H.; Meng, X.; Ke, Y.; Hu, W.; Li, B.; et al. Remote-Triggered Domino-like Cyclodehydrogenation in Second-Layer Topological Graphene Nanoribbons. *J Am Chem Soc* **2023**, *145* (18), 10126-10135. DOI: 10.1021/jacs.3c00563 From NLM PubMed-not-MEDLINE.
(21) Lyu, B.; Chen, J.; Wang, S.; Lou, S.; Shen, P.; Xie, J.; Qiu, L.; Mitchell, I.; Li, C.; Hu, C.; et al. Graphene nanoribbons grown in hBN stacks for high-performance electronics. *Nature* **2024**. DOI: 10.1038/s41586-024-07243-0.
(22) Kolmer, M.; Zuzak, R.; Steiner, A. K.; Zajac, L.; Engelund, M.; Godlewski, S.; Szymonski, M.; Amsharov, K. Fluorine-programmed nanozipping to tailored nanographenes on rutile TiO2 surfaces. *Science* **2019**, *363*, 57-60.
(23) Kolmer, M.; Steiner, A.-K.; Izydorczyk, I.; Ko, W.; Engelund, M.; Szymonski, M.; Li, A.-P.; Amsharov, K. Rational synthesis of atomically precise graphene nanoribbons directly on metal

oxide surfaces. *Science* **2020**, *369*, 571–575.
(24) Richter, A.; Haapasilta, V.; Venturini, C.; Bechstein, R.; Gourdon, A.; Foster, A. S.; Kuhnle, A. Diacetylene polymerization on a bulk insulator surface. *Phys Chem Chem Phys* **2017**, *19* (23), 15172-15176. DOI: 10.1039/c7cp01526g From NLM PubMed-not-MEDLINE.
(25) Palma, C. A.; Diller, K.; Berger, R.; Welle, A.; Bjork, J.; Cabellos, J. L.; Mowbray, D. J.; Papageorgiou, A. C.; Ivleva, N. P.; Matich, S.; et al. Photoinduced C-C reactions on insulators toward photolithography of graphene nanoarchitectures. *J Am Chem Soc* **2014**, *136* (12), 4651-4658. DOI: 10.1021/ja412868w From NLM PubMed-not-MEDLINE.
(26) Fatayer, S.; Moll, N.; Collazos, S.; Perez, D.; Guitian, E.; Pena, D.; Gross, L.; Meyer, G. Controlled Fragmentation of Single Molecules with Atomic Force Microscopy by Employing Doubly Charged States. *Phys Rev Lett* **2018**, *121* (22), 226101. DOI: 10.1103/PhysRevLett.121.226101 From NLM PubMed-not-MEDLINE.
(27) Sun, L.; Zheng, W.; Gao, W.; Kang, F.; Zhao, M.; Xu, W. On-surface synthesis of aromatic cyclo[10]carbon and cyclo[14]carbon. *Nature* **2023**, *623* (7989), 972-976. DOI: 10.1038/s41586-023-06741-x.
(28) Yu, M.; Chen, C.; Liu, Q.; Mattioli, C.; Sang, H.; Shi, G.; Huang, W.; Shen, K.; Li, Z.; Ding, P.; et al. Long-range ordered and atomic-scale control of graphene hybridization by photocycloaddition. *Nature Chemistry* **2020**, *12* (11), 1035-1041. DOI: 10.1038/s41557-020-0540-2.
(29) Zhao, W.; Dong, L.; Huang, C.; Win, Z. M.; Lin, N. Cu- and Pd-catalyzed Ullmann reaction on a hexagonal boron nitride layer. *Chem Commun (Camb)* **2016**, *52* (90), 13225-13228. DOI: 10.1039/c6cc05029h From NLM PubMed-not-MEDLINE.
(30) Summerfield, A.; Baldoni, M.; Kondratuk, D. V.; Anderson, H. L.; Whitelam, S.; Garrahan, J. P.; Besley, E.; Beton, P. H. Ordering, flexibility and frustration in arrays of porphyrin nanorings. *Nat Commun* **2019**, *10* (1), 2932. DOI: 10.1038/s41467-019-11009-y From NLM PubMed-not-MEDLINE.
(31) Zhan, G.; Cai, Z. F.; Strutynski, K.; Yu, L.; Herrmann, N.; Martinez-Abadia, M.; Melle-Franco, M.; Mateo-Alonso, A.; Feyter, S. Observing polymerization in 2D dynamic covalent polymers. *Nature* **2022**, *603* (7903), 835-840. DOI: 10.1038/s41586-022-04409-6 From NLM PubMed-not-MEDLINE.
(32) Daelemans, B.; Bilbao, N.; Dehaen, W.; De Feyter, S. Carbocatalysis with pristine graphite: on-surface nanochemistry assists solution-based catalysis. *Chem Soc Rev* **2021**, *50* (4), 2280-2296. DOI: 10.1039/d0cs01294g From NLM PubMed-not-MEDLINE.
(33) Fabozzi, F. G.; Severin, N.; Rabe, J. P.; Hecht, S. Room Temperature On-Surface Synthesis of a Vinylene-Linked Single Layer Covalent Organic Framework. *Journal of the American Chemical Society* **2023**. DOI: 10.1021/jacs.3c04730.
(34) Niu, W.; Fu, Y.; Serra, G.; Liu, K.; Droste, J.; Lee, Y.; Ling, Z.; Xu, F.; Cojal González, J. D.; Lucotti, A.; et al. Bottom-up Solution Synthesis of Graphene Nanoribbons with Precisely Engineered Nanopores. *Angewandte Chemie International Edition* **2023**, *62* (35). DOI: 10.1002/anie.202305737.
(35) Grossmann, L.; King, B. T.; Reichlmaier, S.; Hartmann, N.; Rosen, J.; Heckl, W. M.; Bjork, J.; Lackinger, M. On-surface photopolymerization of two-dimensional polymers ordered on the mesoscale. *Nat Chem* **2021**, *13* (8), 730-736. DOI: 10.1038/s41557-021-00709-y From NLM PubMed-not-MEDLINE.
(36) Zhang, C.; Kazuma, E.; Kim, Y. Atomic-Scale Visualization of the Stepwise Metal-Mediated

Dehalogenative Cycloaddition Reaction Pathways: Competition between Radicals and Organometallic Intermediates. *Angew Chem Int Ed Engl* **2019**, *58* (49), 17736-17744. DOI: 10.1002/anie.201909111.
(37) Lin, T.; Shang, X. S.; Adisoejoso, J.; Liu, P. N.; Lin, N. Steering on-surface polymerization with metal-directed template. *J Am Chem Soc* **2013**, *135* (9), 3576-3582. DOI: 10.1021/ja311890n From NLM Medline.
(38) Xing, S.; Zhang, Z.; Fei, X.; Zhao, W.; Zhang, R.; Lin, T.; Zhao, D.; Ju, H.; Xu, H.; Fan, J.; et al. Selective on-surface covalent coupling based on metal-organic coordination template. *Nat Commun* **2019**, *10* (1), 70. DOI: 10.1038/s41467-018-07933-0 From NLM PubMed-not-MEDLINE.
(39) Xue, Q.; Xue, N.; Li, J.; Li, Y.; Li, R.; Zhang, Y.; Li, N.; Shen, Z.; Hou, S.; Wang, Y. Self-Assembly of a Metal–Organic Framework by Stepwise Coordination of Carboxyl and Pyrrolyl Groups. *The Journal of Physical Chemistry C* **2020**, *124* (14), 7790-7796. DOI: 10.1021/acs.jpcc.9b11599.
(40) Song, W.; Martsinovich, N.; Heckl, W. M.; Lackinger, M. Thermodynamics of halogen bonded monolayer self-assembly at the liquid-solid interface. *Chem Commun (Camb)* **2014**, *50* (88), 13465-13468. DOI: 10.1039/c4cc06251e.
(41) Han, Z.; Czap, G.; Chiang, C.-l.; Xu, C.; Wagner, P. J.; Wei, X.; Zhang, Y.; Wu, R.; Ho, W. Imaging the halogen bond in self-assembly halogenbenzenes on silver. *Science* **2017**, *358*, 206-210.
(42) Ernst, K. H. Molecular chirality at surfaces. *physica status solidi (b)* **2012**, *249* (11), 2057-2088. DOI: 10.1002/pssb.201248188.
(43) Cai, L.; Gao, T.; Wee, A. T. S. Topology selectivity of a conformationally flexible precursor through selenium doping. *Nature Communications* **2024**, *15* (1). DOI: 10.1038/s41467-024-47614-9.
(44) Zeng, Z.; Guo, D.; Wang, T.; Chen, Q.; Matej, A.; Huang, J.; Han, D.; Xu, Q.; Zhao, A.; Jelinek, P.; et al. Chemisorption-Induced Formation of Biphenylene Dimer on Ag(111). *J Am Chem Soc* **2022**, *144* (2), 723-732. DOI: 10.1021/jacs.1c08284 From NLM PubMed-not-MEDLINE.
(45) Cai, J.; Ruffieux, P.; Jaafar, R.; Bieri, M.; Braun, T.; Blankenburg, S.; Muoth, M.; Seitsonen, A. P.; Saleh, M.; Feng, X.; et al. Atomically precise bottom-up fabrication of graphene nanoribbons. *Nature* **2010**, *466* (7305), 470-473. DOI: 10.1038/nature09211.

Acknowledgements

Y.L.H. acknowledges financial support from the National Natural Science Foundation of China (Grant No.12350610236) and the Natural Science Foundation of Fujian Province (2022J06035). M. Y. acknowledges the funding support from the Hong Kong Polytechnic University (project numbers.: P0034827, P0042711, P0039734, and P0039679), PolyU RCNN (Project No.: P0048122), and Research Grants Council, Hong Kong (project number: 25301523). J.Y. and Y.-W.Z. acknowledge the supports by Italy-Singapore Science and Technology Cooperation (Grant No. R23101R040), and

Singapore A*STAR SERC CRF Award, and the computing resources at the A*STAR Computational Resource Centre and National Supercomputer Centre, Singapore. A.T.S.W acknowledges the support of the National Research Foundation of Singapore CRP26-2021RS-0001.

Competing interests

The authors declare no competing interests.

Table of Content

On-surface synthesis on chemically inert substrates via thermally activation is extremely challenging in ultra-high vacuum (UHV), suffering from a severe "desorption problem". Here, we report an extraordinary side-to-side [2+2+2+2] cycloaddition via dehydrohalogenations occurring in a highly ordered self-assembled molecular array on graphite, where the cycloaddition products are embedded as defective individuals or chains (grain boundaries) even with product density up to ~30%.